Journal of Power Sources 196 (2011) 9561–9567

Contents lists available at ScienceDirect

Journal of Power Sources

journal homepage: www.elsevier.com/locate/jpowsour

Computing approach of cathodic process within solid oxide electrolysis cell: Experiments and continuum model validation

D. Grondin[a,b], J. Deseure[a,*], P. Ozil[a], J.-P. Chabriat[b], B. Grondin-Perez[b], A. Brisse[c]

[a] Laboratoire d'Électrochimie et de Physico-chimie des Matériaux et des Interfaces (LEPMI), UMR 5279 CNRS/Grenoble-INP/UJF/UdS, Phelma/Grenoble INP, 1130 rue de la Piscine, Domaine Universitaire, BP 75, 38402 Saint Martin d'Hères Cedex, France
[b] Laboratoire d'Énergétique, d'Électronique et Procédés (LE2P), EA 4079, 15 avenue René Cassin, BP 7151, 97715 Saint-Denis Messag Cedex 9, France
[c] European Institute For Energy Research (EIFER), Emmy-Noether Strasse 11, D-76131 Karlsruhe, Germany

ARTICLE INFO

Article history:
Received 20 April 2011
Received in revised form 15 June 2011
Accepted 10 July 2011
Available online 5 August 2011

Keywords:
SOEC
Water reduction
Three-electrode techniques
Electrochemical impedance spectroscopy
Continuum model

ABSTRACT

Classical solid oxide fuel cell anode (Ni–cermet) could be employed as solid oxide electrolysis cell cathode. Ni–cermet has been synthesized and tested as solid oxide electrolyzer cathode using three-electrode techniques between 700 °C and 900 °C. yttria stabilized zirconia was used as the electrolyte and Pt as the counter electrode. Polarization curves and impedance spectra have been analyzed for two gas compositions. The presented results demonstrated an influence of Ni–cermet electrode behavior upon gas composition and temperature. The present results highlight a mechanism changing on Ni–cermet electrode upon gas composition. In a second part, a one-dimensional steady state model is developed to predict the cathodic behavior of Ni–cermet. This model takes into account mass and charge conservation, transport of species and reaction kinetics. It considers the porous electrode to be a homogeneous medium characterized. The influence of varying chemical and electrochemical steps kinetic on the shape of polarization curves is discussed. At high overpotential values the model with two rate-limiting steps has been validated using numerical optimization method.

1. Introduction

Significant research efforts are achieved to develop hydrogen economy. Nowadays, industrial mass production of hydrogen is mainly based on hydrocarbons reforming. However water electrolysis could be the most convenient production process if it uses a clean renewable energy source. Solid oxide fuel cells (SOFC) have been intensively investigated during this last decade. Major improvements have been achieved and SOFCs now demonstrate high performance [1]. Solid oxide electrolysis cell (SOEC) has been studied since 1980s as a promising way to produce massively hydrogen [2]. High temperature operation appeared more efficient due to the decreased open circuit voltage and polarization. Using this technology, a low hydrogen production cost is aimed and a recent study indicates that SOEC technology has a promising potential for hydrogen production from renewable energy sources [3]. The cell consists of the assembly of a three-layer region involving two ceramic electrodes separated by a dense ceramic electrolyte made in the same materials as for a SOFC. The hydrogen electrode is usually composed of nickel and yttria-stabilized-zirconia (YSZ) cermet. The electrolyte is made of YSZ and the oxygen electrode is based on perovskite-type oxides, which is usually strontium-doped lanthanum manganite $La_{1-x}Sr_xMnO_3$ (LSM). The properties of these materials were extensively studied and are reasonably known today. However several problems are still unsolved: the electrical and electrochemical stability of materials (electrolytes and interconnects) in both oxidizing and reducing atmospheres and the mechanical stress due to thermal behavior of SOEC. More interest arises for SOEC with the recent breakthrough in SOFC technology and the investigation of reversible SOFC [4]. Most SOEC studies are carried out with the same cell as SOFC in order to benefit of a reversible system able to convert both hydrogen to electricity (power generation) and electricity to hydrogen (energy storage) [5,6]. However performance still remains limited in electrolysis mode compared to fuel cell one [7].

To provide a better comprehension of electrochemical process, literature reports at least two testing methods. The first one consists in testing SOEC under different operating conditions at a single electrode. However it is impossible to obtain any polarization curve of the electrode and to perform any electrochemical kinetic study. On the contrary the second method, called three-electrode technique which involves a reference electrode located at a suitable place, allows such study [8]. Polarization curves are not sufficiently relevant to determine either the limiting processes or

* Corresponding author. Tel.: +33 04 76 82 65 86; fax: +33 04 76 82 67 77.
E-mail address: Jonathan.Deseure@lepmi.grenoble-inp.fr (J. Deseure).

0378-7753/$ – see front matter © 2011 Elsevier B.V. All rights reserved.
doi:10.1016/j.jpowsour.2011.07.033

Nomenclature

av_{ads}	specific adsorption area (m^{-1})
av_{TPB}	specific electrochemical area (m^{-1})
C_{dl}	double layer capacity ($F\,m^{-2}$)
C_i	concentration of specie i ($mol\,m^{-3}$)
$C_{i,0}$	concentration of specie i in the gas channel ($mol\,m^{-3}$)
d_g	mean grain diameter (m)
$D_{i,j}^{eff}$	effective molecular diffusion coefficient ($m^2\,s^{-1}$)
$D_{k,i}$	Knudsen diffusion coefficient ($m^2\,s^{-1}$)
d_p	mean pore diameter (m)
F	Faraday constant (=96,485 $C\,mol^{-1}$)
J_{cell}	three-electrode cell current density ($A\,cm^{-2}$)
k_{ads}	adsorption kinetic constant ($Pa^{-1}\,s^{-1}$)
k_{des}	desorption kinetic constant (s^{-1})
$k_{1/-1}$	kinetic constant ($m^2\,s^{-1}\,mol^{-1}$)
k_i	kinetic constant (s^{-1})
L	electrode thickness (m)
M_i	molecular weight ($g\,mol^{-1}$)
N_i	molar flux ($mol\,s^{-1}\,m^{-2}$)
n_j	number of electrons exchanged at the jth step
P	pressure (Pa)
P_i	partial pressure (Pa)
R	gas constant (=8.314 $J\,K^{-1}\,mol^{-1}$)
v_i	surface reaction kinetic ($mol\,s^{-1}\,m^{-2}$)
T	temperature (K)
y_i	molar fraction
α	symmetrical factor
ε	porosity
ϕ_{cM}	potential of the electron conducting phase (V)
ϕ_{cS}	potential of the ionic conducting phase (V)
η	electrode overpotential (V)
φ_i	volume fraction
v_i	rate of the ith step ($mol\,m^{-3}$)
θ	coverage of adsorbed OH^-
θ_2	coverage of adsorbed H_2O
σ^{eff}	effective conductivity ($S\,m^{-1}$)
σ	ionic or electronic conductivity ($S\,m^{-1}$)
τ	gas phase tortuosity
τ_s	solid phase tortuosity
Γ	maximal adsorbed specie concentration ($mol\,m^{-2}$)

the reaction mechanism. Thus, another technique, electrochemical impedance spectroscopy (EIS) is used to identify and characterize the various phenomena involved in electrode reactions in order to optimize the entire process [9,10]. Concerning the hydrogen electrode, Ni–cermet was shown to offer poorer performance in SOEC mode than in SOFC mode. Under high steam concentration, Ni–cermet degrades for low hydrogen content in the gas [4,7]. However, some previous investigations performed at $T = 1000\,^{\circ}C$ with a P_{H_2O}/P_{H_2} ratio = 10 demonstrated that nickel electrode exhibits attractive performances in high temperature electrolysis operation. Schouler et al. [11] suggest several possible reaction schemes for water electroreduction depending on the overpotential region. For low overpotentials, a direct electrochemical water reduction is assumed whereas for high overpotentials electrolyte redox couple seems to participate to water reduction. According to Eguchi et al. [4] the mechanism of steam reduction does not only depend on electrode material; temperature and moisture partial pressure appear to be critical parameters of electrochemical reaction. Marina et al. [7] present Tafel's parameters for different experimental conditions. Ni–cermet cathodic polarizations exhibit a transport-controlled behavior. However the hydrogen electrode is less studied than the oxygen one because it is assumed that the major limitation comes from the anode side in electrolysis mode [12].

Computing simulation appears to be one of the most efficient approaches to analyze the coupled mechanisms of SOEC operation. Modeling of SOFC electrodes could be focused on optimization or characterization [13]. It opens the possibility of testing the influence of parameters such as: intrinsic conductivities, particle size, graded or homogeneously distributed porosity or composition [14]. The model employed should depend on which type of loss dominates, on operating conditions and other parameters such as microstructure or intrinsic conductivities [15,16]. Nevertheless, few works are available in literature regarding the water reduction kinetic on Nickel/YSZ cermet. Two electrochemical models were developed for an electrolyte supported cell and simulations were compared to experimental data [17,18]. Both models seem to provide quite accurate predictions although there are different. Only one theoretical study was proposed for a cathode-supported SOEC, but without any comparison with experimental data [19]. The major part of available models uses a Butler–Volmer's law for activation overpotential calculation. However, this approach seems to be not precise enough. In our previous work [20], it has been emphasized that a more accurate electrochemical model for water reduction is required to describe the high current density operation at low inlet water concentration.

In this study, Ni–cermet is synthesized and tested as solid oxide electrolyzer cathode using three-electrode technique. YSZ is used as the electrolyte and Pt as the counter electrode. The experimental part is focused on the behavior of cathodic Ni–cermet polarization in 3%H_2O/H_2 and 3%H_2O–3%H_2/N_2 between 700 °C and 900 °C with EIS measurement. Polarization curves and impedance spectra have been analyzed for different gas compositions. Indeed, several capacitive contributions have been recorded depending on gas composition, temperature and current density. In the modeling part, a continuum model is proposed for a porous composite cathode (Ni–YSZ cermet). It provides a complete description of the electrode structure and the processes occurring therein accounting for activation, mass and charge transports. The Ni–cermet manufactured in this work has been characterized to provide the classical parameters of microstructure (porosity, mean grain diameters) used in the computational approach. Kinetic parameter value of electrochemical and chemical reactions are fitted using numerical optimization method. Predictions from simulations are compared to experimental results. The model could exhibit the polarization curves with one or two electrochemical or chemical steps occurred in water reduction. From this observation, one of the proposed water reduction processes is selected to predict the cell electrical behavior in steady state.

2. Experimental part

2.1. Sample preparation and characterization

A commercial Ni carbonate powder (Acros Organics) was used as NiO precursor. $CH_4Ni_3O_7{\cdot}xH_2O$ was calcined at 1000 °C for 1 h to obtain pure NiO. Hydrogen electrode ink was prepared using 40 wt.% NiO, 60 wt.% YSZ powders and the right amount of ethylene glycol. A 20 mm diameter and 2 mm thickness dense YSZ pellet (Tosoh, 8 mol.% yttria) was used as the electrolyte. The ink was sprayed over the substrate using a 3D robot spray coater, insuring a good control of electrode thickness. A Pt ink was used to make the counter electrode (CE) and a Pt wire as the reference electrode (RE). This electrode was located at a distance close to half the electrolyte thickness.

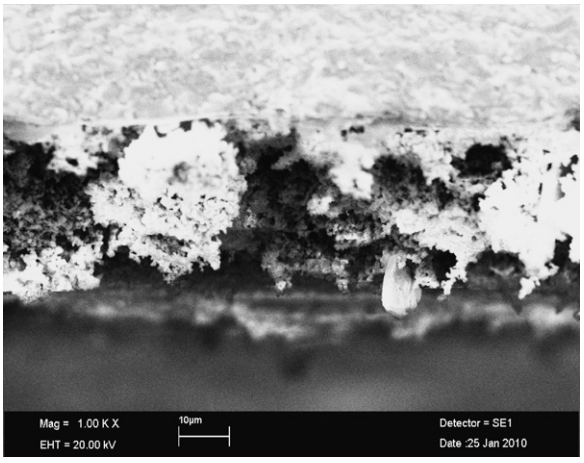

Fig. 1. Scanning electron micrograph of the cross-section of electrolyte/Ni–YSZ cermet.

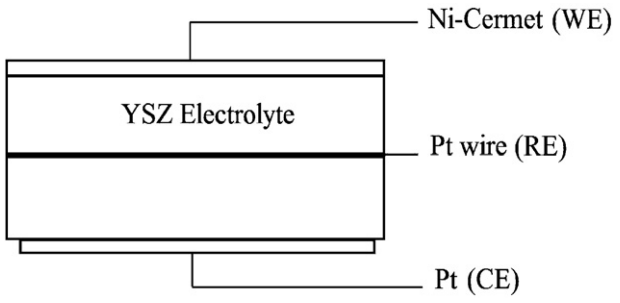

Fig. 2. Schematic view of the experimental three-electrode cell.

A thickness of 32 μm for the Ni–YSZ cermet electrode is estimated from scanning electron micrographs. Image shows homogenous grain size throughout the electrode (Fig. 1). One may note presence of aggregates which confirm that the electrode is not optimized for high performance. Indeed, the goal of this study is to have a better understanding of charge transfer processes.

2.2. Electrochemical characterizations

The setup for electrochemical measurement is schematized in Fig. 2. The Ni–YSZ/YSZ/Pt cell was fed with either 3%H_2O/H_2 at 2.6×10^{-3} N m^3 h^{-1} or 3%H_2O–3%H_2/N_2 at 1.3×10^{-3} N m^3 h^{-1}. Steam generator is a gas bubbler at room temperature. Before measuring, the working electrode is reduced with dry hydrogen during 24 h at 800 °C. All trials were performed at atmospheric pressure. The electrodes were connected to a Solartron 1260 for impedance and *I–V* measurements. Impedance measurements were performed scanning from 0.1 Hz to 65 kHz with applied amplitude of 10 mV.

In the present work, the three-electrode cell enabled us to determine the working overpotential at several points of the *I–V* curve. Impedance measurements were also carried out at various intensities. These measurements allow us correcting the errors arising from a shift in the electrolyte current distribution from the primary to the secondary current distribution under load [8].

3. Results and discussion

Fig. 3 shows polarization losses in the Ni–YSZ electrode. Below 800 °C the lowest overpotentials have been recorded for a same magnitude of current density within $PH_2O/PH_2 = 1$. At 800 °C and higher temperatures, it has been recorded for a steam/hydrogen ratio of 0.03. These results are in agreement with Eguchi et al. [4] studies.

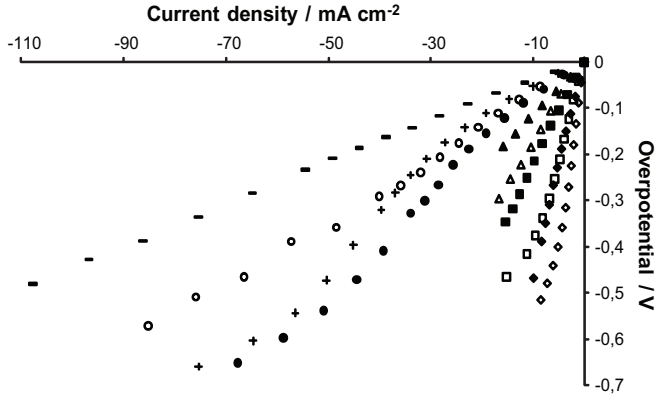

Fig. 3. Polarization curves of the working electrode, Ni–YSZ for $P_{H_2O}/P_{H_2} = 1$ at 700 °C (♦), 750 °C (■), 800 °C (▲), 850 °C (●) and 900 °C (+) and 0.03 at 700 °C (◊), 750 °C (□), 800 °C (△), 850 °C (○) and 900 °C (—).

The main experimental results are gathered in Table 1. It appears that for low water content the electrochemical behavior is clearly dissimilar between 800 °C and 900 °C. From 700 °C to 800 °C the impedance diagrams involve only two capacitive contributions while three capacitive contributions should be presented at 900 °C. In addition the apex frequencies of the first capacitive contribution increase from 2 kHz to 5 kHz with temperature except at 900 °C where the apex frequency is equal to 2 kHz. Reaction kinetic is proportional to the apex frequencies, then until 800 °C the charge transfer is enhanced by temperature effect. At 900 °C, the charge transfer seems to be inhibited by the apparition of a lower charge transfer process since there is more than one contribution in low frequency range. In addition, observation is completely different at 900 °C as shown by the changing shapes of impedance spectra at this temperature as shown in Fig. 4. The impedance diagram shapes and the apex frequencies depend on steam/hydrogen ratio and load. The electrode is less impedent for a steam/hydrogen ratio of 1 than it is for 0.03. The water effect on the electrocatalytic activity is thus clearly pointed out by this figure. Our results are in agreements with Schouler et al. investigations stating that the transition

Table 1
Apex frequencies.

T	$P_{H_2O}/P_{H_2} = 0.03$		$P_{H_2O}/P_{H_2} = 1$	
	J_{cell} = 8.6 mA cm^{-2} for η = 520 mV		J_{cell} = 8.4 mA cm^{-2} for η = 390 mV	
700 °C	1st contribution	2.3 kHz	1st contribution	1.6 kHz
	2nd contribution	85 Hz	2nd contribution	260 Hz
T	$P_{H_2O}/P_{H_2} = 0.03$		$P_{H_2O}/P_{H_2} = 1$	
	J_{cell} = 11.3 mA cm^{-2} for η = 420 mV		J_{cell} = 15.4 mA cm^{-2} for η = 360 mV	
750 °C	1st contribution	3.4 kHz	1st contribution	3.4 kHz
	2nd contribution	65 Hz	2nd contribution	360 Hz
T	$P_{H_2O}/P_{H_2} = 0.03$		$P_{H_2O}/P_{H_2} = 1$	
	J_{cell} = 16.7 mA cm^{-2} for η = 297 mV		J_{cell} = 16 mA cm^{-2} for η = 380 mV	
800 °C	1st contribution	4 kHz	1st contribution	5 kHz
	2nd contribution	160 Hz	2nd contribution	600 Hz
T	$P_{H_2O}/P_{H_2} = 0.03$		$P_{H_2O}/P_{H_2} = 1$	
	J_{cell} = 75.4 mA cm^{-2} for η = 300 mV		J_{cell} = 64.7 mA cm^{-2} for η = 600 mV	
900 °C	1st contribution	2 kHz	1st contribution	2 kHz
	2nd contribution	650 Hz	2nd contribution	500 Hz
	3rd contribution	7 Hz	3rd contribution	3.5 Hz

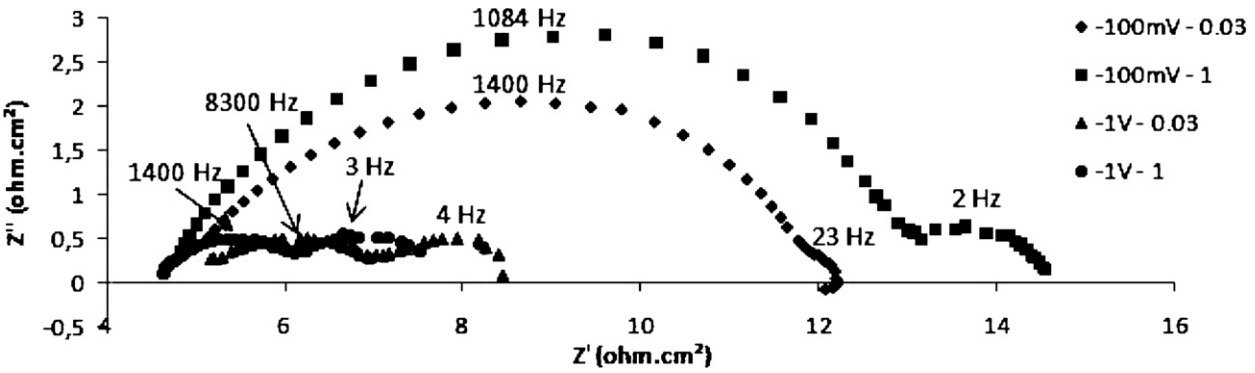

Fig. 4. Impedance spectra for a working electrode potential of −100 mV and −1 V/ref with steam/hydrogen ratio of 0.03 and 1 at 900 °C.

between the varying mechanisms depends on operating temperature, gas composition and applied potential [11]. At 900 °C, for a difference of −1 V between the working and the reference electrode (−1 V/ref), the low frequency contributions have the same amplitude as high frequency contributions for both ratios. First the low frequency contribution could be assign to a diffusion process. But this assumption is not in agreement with the small current densities recorded in these experiments and the absence of nitrogen for $P_{H_2O}/P_{H_2} = 0.03$ does not involves a lower amplitude of this capacitive contributions. A simple diffusion process could not explain this behavior. These results emphasize the possible existence of coupled processes.

3.1. Theoretical assumption of reduction process from literature

According to literature, two kinds of reaction mechanisms have been suggested on Ni–YSZ interfaces [11,21]. For a nickel electrode at low P_{H_2O} the mechanism could correspond to the following reactions:

$$H_2O_{gas} + O^{2-}_{TPB} \rightarrow 2OH^-_{ads} \quad (1)$$

$$V_O^{\bullet\bullet} + OH^-_{ads} + e^- \rightarrow O^X_O + (1/2)H_2 \quad (2)$$

and the corresponding kinetics equation could be expressed as following [22]:

$$\nu_1 = k_1\,\Gamma^2 \exp\left(\frac{\alpha F}{RT}(\phi_{cM} - \phi_{cS})\right)\,\theta^2 - k_{-1}\Gamma^2 \times \exp\left(-\frac{(1-\alpha)F}{RT}(\phi_{cM} - \phi_{cS})\right)(1-\theta)^2\left(\frac{C_{H_2O}}{C_{H_2O,0}}\right) \quad (3)$$

$$\nu_2 = k_2\Gamma \exp\left(\frac{\alpha F}{RT}(\phi_{cM} - \phi_{cS})\right)\left(\frac{C_{H_2}}{C_{H_2,0}}\right)^{1/2}(1-\theta) - k_{-2}\,\Gamma \times \exp\left(-\frac{(1-\alpha)F}{RT}(\phi_{cM} - \phi_{cS})\right)\theta \quad (4)$$

At high steam pressure, a direct reduction of steam has been demonstrated. The mechanism could then be expressed as:

$$H_2O_{gas} \rightarrow H_2O_{ads} \quad (5)$$

$$V_O^{\bullet\bullet} + H_2O_{ads} + 2e^- \rightarrow O^X_O + H_2 \quad (6)$$

The kinetics of steam adsorption and reduction being similar to oxygen kinetics in SOFC mode [13] may be described by:

$$\nu_3 = \Gamma_2 k_{ads} P_{H_2O}(1-\theta_2) - \Gamma_2 k_{des}\theta_2 \quad (7)$$

$$\nu_4 = k_4\Gamma_2 \exp\left(\frac{\alpha 2F}{RT}(\phi_{cM} - \phi_{cS})\right)\frac{C_{H_2}}{C_{H_2,0}}(1-\theta_2) - k_{-4}\Gamma_2 \times \exp\left(-\frac{(1-\alpha)2F}{RT}(\phi_{cM} - \phi_{cS})\right)\theta_2 \quad (8)$$

The rates of steps (ν_i) depend on hydrogen or steam concentration and on coverage of adsorbed species (θ for OH^- or θ_2 for H_2O) with kinetic constants ($k_{\pm i}$). According to Schouler et al., the transition between the two mechanisms appears close to – 1.2 V/air for Ni–YSZ [11]. Moreover, this transition also depends on operating conditions (temperature, gas composition) such as observed in Table 1. The presented experimental results do not permit to select a mechanism as a function of temperature or P_{H_2O}/P_{H_2} ratio. Klein et al. have emphasized that the overpotential are not homogenous within the porous electrode due to the material electric conductivity [23]. Then, it is quite possible that both electrochemical ways exist.

In other hand, some limitations due to an electronic conductivity of the YSZ should appear in SOEC mode. According to Pham and Glass [24], an electronic conduction due to partial electrolysis of the electrolyte should occur for an oxygen pump. However, this effect at "high enough polarization" (e.g. 10^{-15} atm at 800 °C) is still much higher than values reported by Yuan and Kröger (10^{-27} atm) [25]. Subsequently, in the context of SOEC, it was reported at high concentration polarization losses, possible electronic short-circuit within the electrolyte [26].

Although in SOEC mode, the cermet assumes a cathodic polarization which protects the nickel material. Accorsi and Bergmann [27] have suggested that steam partial pressure in SOEC mode must be less than 20% to avoid the nickel oxidation. And, it is established that the nickel could be not oxidized if the H_2 composition is higher than 2% at 900 °C [28]. The possible re-oxidation process of cermet involves a degradation of the hydrogen electrode [29] and the risk of Ni re-oxidation increases with decreasing Ni grain size, the gradient of overpotential and steam composition through the electrode. So, the possible reduction of YSZ and re-oxidation of Ni should impact the electrochemical process of steam reduction.

4. Modeling part

4.1. Continuum model

The continuum model [13] is isothermal and one-dimensional (Fig. 5). It is assumed that the gas partial pressure, concentration of gaseous and adsorbed species and overpotential are uniform over the geometrical surface area of the electrode. Ohmic losses in the well-connected electronic conductor phase are neglected. Thus,

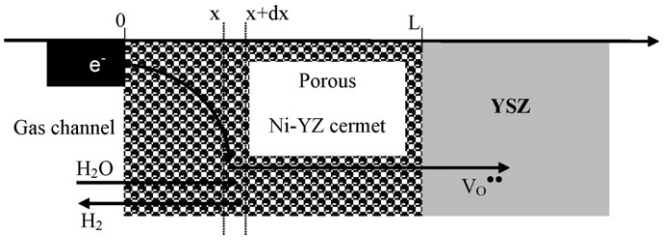

Fig. 5. Schematic representation of porous Ni–YSZ cermet electrode.

this phase is regarded as equipotential. Transport of oxygen vacancies in YSZ is strictly ohmic. In the case under study, water steam is provided with hydrogen and in some conditions with nitrogen. Stefan–Maxwell diffusion model [30] is used regarding the significant difference between molecular weight of species. Moreover, Knudsen diffusion [31] should be considered in the electrode that is a porous media. Thus, the Dusty-Gas Model (DGM) is used at cathode. Such model seems to provide the most accurate description of mass transport for SOFC anode [32].

Molar fraction variation of specie i $y_i(x, t)$ is calculated solving the following equation:

$$\frac{\partial y_i}{\partial x} = \frac{RT}{P}\left(\sum_j \left[\frac{y_i N_j - y_j N_i}{D_{ij}^{eff}}\right] - \frac{N_i}{D_{k,i}}\right) \tag{9}$$

The Knudsen diffusion coefficient of the species i ($D_{k,i}$) is calculated from relation (Eq. (10)) where the mean pore diameter is determined considering electrode characteristics (Eq. (11)).

$$D_{k,i} = d_p \frac{\varepsilon}{3\tau}\sqrt{\frac{8RT}{\pi M_i}} \tag{10}$$

$$d_p = \frac{2}{3}\frac{\varepsilon}{1-\varepsilon} d_g \tag{11}$$

The effective diffusion coefficient is the diffusion coefficient in a porous media. Different models were used to assess this coefficient [33,34]. Our models developed for SOEC cathode use the Bruggeman's law.

$$D_{i,j}^{eff} = D_{i,j}\varepsilon^{\tau} \tag{12}$$

Mass conservation for each species could be written as follows:

$$\frac{\partial N_{H_2}}{\partial x} \pm a v_{TPB}\sum_j v_j = \frac{P}{RT}\frac{\partial y_{H_2}}{\partial t} \tag{13}$$

$$\frac{\partial N_{H_2O}}{\partial x} \pm a v_{TPB}\sum_j v_j = \frac{P}{RT}\frac{\partial y_{H_2O}}{\partial t} \tag{14}$$

$$\frac{\partial N_{N_2}}{\partial x} = \frac{P}{RT}\frac{\partial y_{N_2}}{\partial t} \tag{15}$$

Total pressure is assumed to be constant then one can consider the following condition:

$$\sum_i y_i = 1 \tag{16}$$

Molar fractions are known at $x = 0$. At $x = L$, flux are nil. Diffusion of adsorbed species, OH^-_{ads} et H_2O_{ads} are assumed to be negligible compared to diffusion process in the gas phase since diffusion coefficients of the adsorbed species are on the order of 10^{-12} m^2 s^{-1} [35]. Thus, mass balance becomes:

$$a v_{ads}\Gamma_i \frac{\partial \theta_i}{\partial t} = \pm\sum_j v_j \tag{17}$$

The overpotential (η) is equal to the difference between potential of the electron conducting phase and the potential of the ionic conducting phase. Then, continuity equation related to faradic process and double-layer charging process is given by:

$$a v_{TPB} C_{dl}\frac{\partial \eta}{\partial t} - \frac{\partial^2(\sigma^{eff}\eta)}{\partial x^2} + a v_{TPB} F\sum_j n_j r_j = 0 \tag{18}$$

$a v_{TPB}$ is specific electrochemical area which represents electrochemically active surface per unit volume of electrode. This area could be estimated from statistic law of binary mixture powder [36,37]. Assuming a one rate-limiting step, the Butler–Volmer law can be used to describe the kinetic as demonstrated for the Volmer–Heyrovsky mechanism [38]. A parametric study revealed a similar behavior for the global and the approximated kinetics. For calibration and validation steps, the electrochemical kinetic has been described by the following equation:

$$v_{2bis} = k_{2bis}\exp\left(\frac{\alpha_a F}{RT}\eta\right)\left(\frac{C_{H_2}}{C_{H_2,0}}\right)^{1/2} - k_{-2bis} \times \exp\left(-\frac{\alpha_c F}{RT}\eta\right)\left(\frac{C_{H_2O}}{C_{H_2O,0}}\right) \tag{19}$$

Electrode is a composite of electronic and ionic conductors. Effective electronic and ionic conductivities are estimated by the following relation [39]:

$$\sigma_{el\ or\ io}^{eff} = \varphi_{Ni\ or\ YSZ}\frac{1-\varepsilon}{\tau_s}\sigma_{Ni\ or\ YSZ} \tag{20}$$

Ionic conductivity of the YSZ is considered as temperature dependent by the equation [40]:

$$\sigma_{YSZ} = 0.334 \times 10^5 \exp\left(-\frac{10,300}{T}\right) \tag{21}$$

Nickel electronic conductivity is taken as a constant since its variation on the studied temperature range is negligible. A value of 6.5×10^4 S m^{-1} has been considered [41]. A potential is set at the electrode/electrolyte interface and Ionic current is nil at the gas channel/electrode interface ($x = 0$).

$$\eta_{(x=L)} = \eta^L \tag{22}$$

$$\left.\frac{d\eta}{dx}\right|_{x=0} = 0 \tag{23}$$

In steady-state, mass balances are solved using Runge–Kutta method and charge balance using Newton–Raphson in-house developed.

4.2. Simulation results

The continuum model has been solved to generate polarization curves. First, kinetics parameters have been determined in a calibration step. During this step, the least square distance between the model and the experimental data are minimized. This parametric optimization has been carried out using the simplex method

Table 2
Parameter value used for the calibration step.

Parameter	Value	Unit	Reference
τ_s	1.7	–	[13]
τ	4.8	–	[20]
d_g	1×10^{-6}	m	This study
ε	0.3	–	This study
φ_{YSZ}	0.6	–	This study
α	0.5	–	[7]

Table 3
Kinetics parameters obtained from the calibration step.

P_{H_2O}/P_{H_2}	$av_{TPB}k_{2bis}$	$av_{TPB}k_{-2bis}$	$av_{TPB}k_4\Gamma_2$	$av_{TPB}k_{-4}\Gamma_2$	$av_{ads}\Gamma_2 k_{ads}$	$av_{ads}\Gamma_2 k_{des}$
0.03	79.2	2.38	7.47×10^6	770	1.34×10^5	4.03×10^7
1	239	239	1.22×10^7	2.17×10^6	2.16×10^5	8.89×10^7

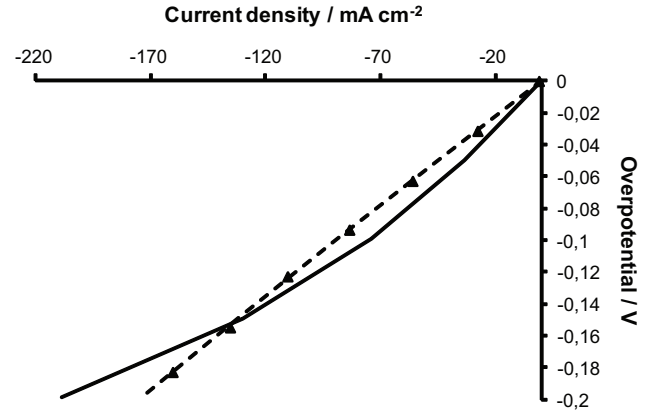

Fig. 6. Comparison between experimental (▲) and simulated polarization curves considering an adsorbed water molecule (- - -) or an adsorbed hydroxide ion (—) in the reaction path under a P_{H_2O}/P_{H_2} of 0.03 at 800 °C.

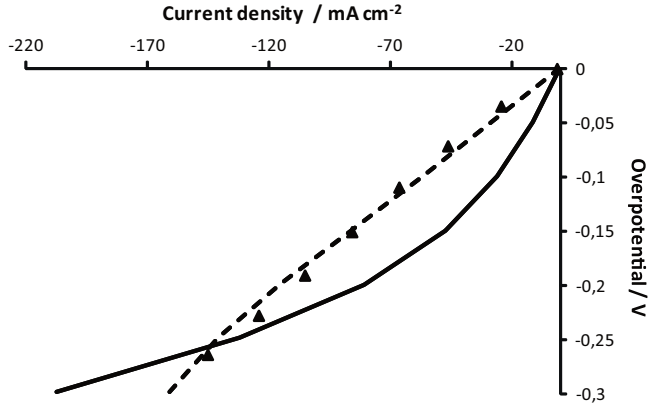

Fig. 7. Comparison between experimental (▲) and simulated polarization curves considering an adsorbed water molecule (- - -) or an adsorbed hydroxide ion (—) in the reaction path under a P_{H_2O}/P_{H_2} of 1 at 800 °C.

available in Matlab®. In order to avoid a too large number of parameter, some of them are estimated. Considered values are gathered in Table 2.

Kinetics parameters determined with the simplex method are given in Table 3. The best fit is obtained for the model where an adsorbed water molecule is involved in the reaction path (see Figs. 6 and 7). The other reaction path (Eqs. (1) and (2)) has been modeled using the Butler–Volmer equation assuming one rate-limiting step. The disagreement observed in Figs. 6 and 7 leads to the conclusion that this equation is not adapted to model the electrochemical behavior of the electrode for the considered gas compositions.

Comparison between simulation and experimental data leads to the conclusion that there is more than one rate-limiting step reaction for water reduction. The cathodic reaction takes place at the triple phase boundaries described by the av_{TPB} coefficient of specific electrochemical area. In this study the in-house cermet exhibits large aggregates which involve small specific reaction areas av_{TPB} and $av_{ADS}\Gamma_2\, k_{des}$. These small performances involve a high magnitude of ASR and make easy the identifications of varying contribution. The kinetics of steam adsorption $av_{ADS}\Gamma_2\, k_{ads}$, steam desorption $av_{ADS}\Gamma_2\, k_{des}$ and reduction are restrained in the same magnitude values under both studied atmospheres. Nevertheless, it is worthy to note the significant scale change of the fitted value for the oxidation kinetics $av_{TPB}k_{-4}\,\Gamma_2$ from 770 mol s^{-1} m^{-3} at $P_{H_2O}/P_{H_2} = 0.03$ to 2.17×10^6 mol s^{-1} m^{-3} at $P_{H_2O}/P_{H_2} = 1$. Then, our investigations are in agreement with the observations of Sukeshini et al. who highlighted a strong difference of electrochemical behavior between anodic and cathodic polarizations of Ni–YSZ cermet [42]. The definition of the transfer current density in macro-scale model should be reconsidered in the light of this result. Another equation should be defined taking into account for example an adsorption step.

5. Conclusion

In this study, a Ni–cermet electrode has been electrochemically characterized using the three-electrode technique. Polarization curves and impedances measurements have been carried out for temperature between 700 °C and 900 °C for two gas compositions. The influence of water activity on electrode behavior has been pointed out. The electrochemical behavior of the Ni–cermet depends on temperature and steam/hydrogen ratio. For temperatures below 900 °C and steam content close to 3 vol.%, the polarization curves exhibit lower overpotential with a steam/hydrogen of 1 than 0.03. Moreover the electrochemical impedance spectra show a low frequency contribution, but the diffusion processes which are classically attributed at this range of frequency are not valid due to low current densities recorded. In the second part of this work, a continuum model has been developed. Two different mechanisms have been studied for the mass and charge transfer. The first one has been modeled assuming one rate-limiting step. This assumption used to justify Butler–Volmer equation does not permit relevant computing predictions of polarization curves. Therefore, the Butler–Volmer description is not valid to model water reduction on Ni–cermet for this water content. The mechanism considering the adsorption of water molecule seems to be the most plausible. When two rate-limiting steps are modeled, comparisons between simulated polarization curves and experimental ones have a good agreement.

Acknowledgment

The author would like to kindly acknowledge Pr. Laurent Dessemond for letting us use its facilities.

References

[1] P.K. Cheekatamarla, C.M. Finnerty, Y. Du, J. Jiang, J. Dong, P.G. Dewald, C.R. Robinson, J. Power Sources 188 (2009) 521–526.
[2] W. Doenitz, R. Schmidberger, E. Steinheil, R. Streicher, Int. J. Hydrogen Energy 5 (1980) 55–63.
[3] S.J. Jensen, P.H. Larsen, M. Mogensen, Int. J. Hydrogen Energy 32 (2007) 3253–3257.
[4] K. Eguchi, T. Hatagishi, H. Arai, Solid State Ion. 86–88 (1996) 1245–1249.
[5] M. Liang, B. Yu, M. Wen, J. Chen, J. Xu, Y. Zhai, J. Power Sources 190 (2009) 341–345.
[6] C.-G. Fan, T. Iida, K. Murakami, T. Matsui, R. Kikuchi, K. Eguchi, J. Fuel Cell Sci. Technol. 5 (2008) 031202/1–031202/5.
[7] O.A. Marina, L.R. Pederson, M.C. Williams, G.W. Coffey, K.D. Meinhardt, C.D. Nguyen, E.C. Thomsen, J. Electrochem. Soc. 154 (2007) B452–B459.

[8] G.J. Offer, P. Shearing, J.I. Golbert, D.J.L. Brett, A. Atkinson, N.P. Brandon, Electrochim. Acta 53 (2008) 7614–7621.
[9] E.P. Murray, S.A. Barnett, Solid State Ion. 143 (2001) 265–273.
[10] S.P. Jiang, J.G. Love, Y. Ramprakash, J. Power Sources 110 (2002) 201–208.
[11] E.J.L. Schouler, M. Kleitz, E. Forest, E. Fernandez, P. Fabry, Solid State Ion. 5 (1981) 559–562.
[12] W. Wang, Y. Huang, S. Jung, J.M. Vohs, R.J. Gorte, J. Electrochem. Soc. 153 (2006) A2066–A2070.
[13] J. Deseure, Y. Bultel, L. Dessemond, E. Siebert, Electrochim. Acta 50 (2005) 2037–2046.
[14] J. Deseure, Y. Bultel, L.C.R. Schneider, L. Dessemond, C. Martin, J. Electrochem. Soc. 154 (2007) B1012–B1016.
[15] C.W. Tanner, K.-Z. Fung, A.V. Virkar, J. Electrochem. Soc. 144 (1997) 21–30.
[16] A.V. Virkar, J. Chen, C.W. Tanner, J.-W. Kim, Solid State Ion. 131 (2000) 189–198.
[17] M. Ni, M.K.H. Leung, D.Y.C. Leung, Chem. Eng. Technol. 29 (2006) 636–642.
[18] M. Ni, M.K.H. Leung, D.Y.C. Leung, Electrochim. Acta 53 (2007) 6707–6718.
[19] J. Udagawa, P. Aguiar, N.P. Brandon, J. Power Sources 166 (2007) 127–136.
[20] D. Grondin, J. Deseure, A. Brisse, M. Zahid, P. Ozil, J. Appl. Electrochem. 40 (2010) 933–941.
[21] A. Hammou, in: B.V.R. Chowdari (Ed.), Advanced Materials for Emerging Technologies, Proceedings of the 10th Asian Conference on Solid State Ionics, World Scientific, 2006, p. 85.
[22] A.J. Bard, L.R. Faulkner, Electrochemical Methods Fundamentals and Applications, Wiley, New York, 1980.
[23] J.-M. Klein, Y. Bultel, M. Pons, P. Ozil, J. Appl. Electrochem. 38 (2008) 497–505.
[24] A.Q. Pham, R.S. Glass, Electrochim. Acta 43 (1998) 2699–2708.
[25] D. Yuan, F.A. Kröger, J. Electrochem. Soc. 116 (1969) 594–600.
[26] J. Schefold, A. Brisse, M. Zahid, J. Electrochem. Soc. 156 (2009) 897–904.
[27] R. Accorsi, E. Bergmann, J Electrochem. Soc. 127 (1980) 804–811.
[28] J.F. Elliott, M. Gleiser, Thermochemistry of Steel Making, vol. 1, Addison-Wesley, New York, 1960.
[29] D. Waldbillig, A. Wood, D.G. Ivey, J. Power Sources 145 (2005) 206–215.
[30] W. Lehnert, J. Meusinger, F. Thom, J. Power Sources 87 (2000) 57–63.
[31] S. Sunde, J. Electroceram. 5 (2000) 153–182.
[32] R. Suwanwarangkul, E. Croiset, M.W. Fowler, P.L. Douglas, E. Entchev, M.A. Douglas, J. Power Sources 122 (2003) 9–18.
[33] F.G. Ho, W.J. Strieder, J. Chem. Phys. 73 (1980) 6296–6300.
[34] D. Mu, Z.S. Liu, C. Huang, N. Djilali, J. Porous Mater. 14 (2007) 49–54.
[35] S.B. Adler, Solid State Ion. 111 (1998) 125–134.
[36] P. Costamagna, P. Costa, V. Antonucci, Electrochim. Acta 43 (1998) 375–394.
[37] S.H. Chan, Z.T. Xia, J. Electrochem. Soc. 148 (2001) A388–A394.
[38] A.J. Bard, L.R. Faulkner, Electrochimie, Principes, Méthodes et Applications, Masson, Paris, 1983.
[39] J. Deseure, Y. Bultel, L. Dessemond, E. Siebert, P. Ozil, J. Appl. Electrochem. 37 (2007) 129–136.
[40] P. Aguiar, C.S. Adjiman, N.P. Brandon, J. Power Sources 138 (2004) 120–136.
[41] D. Simwonis, F. Tietz, D. Stöver, Solid State Ion. 132 (2000) 246–251.
[42] A.M. Sukeshini, B. Habibzadeh, B.P. Beker, C.A. Stoltz, B.W. Eichhorn, G.S. Jackson, J. Electrochem. Soc. 153 (2006) A705–A715.